A Model of *Mesodinium Rubrum* Blooms in the Columbia River Estuary

by

Elisabeth J. Sherry

A PROJECT

submitted to

Oregon State University

University Honors College

in partial fulfillment of
the requirements for the
degree of

Honors Baccalaureate of Science in Chemical Engineering
(Honors Scholar)

Presented May 22, 2015
Commencement June 2015

AN ABSTRACT OF THE THESIS OF

Elisabeth J. Sherry for the degree of Honors Baccalaureate of Science in Chemical
Engineering presented on May 22, 2015. Title: A Model of *Mesodinium Rubrum* Blooms
in the Columbia River Estuary

Abstract approved: _____
Yvette H. Spitz

Every year in the late summer, patches of the Columbia River estuary begin to turn red.
These patches are blooms of mixotrophic ciliates (*Myrionecta rubra* or *Mesodinium
rubrum/major*) (MR) that ingest the chloroplast of their prey, the cryptophytes (CR)
Teleaulax amphioxeia (Peterson et al., 2013), and use the acquired organs to photosynthesize.
The ecological cues that trigger this bloom and its impact on the estuary biogeochemistry are
not fully understood. A one-dimensional five-component ecosystem model was applied and
tested in a MATLAB framework. This paper describes sensitivity analyses of the model with
respect to nitrate advection, MR and CR maximum uptake and mortality rates, and the rate of
MR photosynthesis. The impact of vertical migration and the importance of the seed
population were also considered. A set of parameters was selected to produce an optimal
surface bloom of MR and CR comparable to the one observed in the chlorophyll-a and
phycoerythrin measured at the south channel endurance station, SATURN 03, in 2010. Most
of the parameters are positively correlated with the MR and CR bloom timing, duration, and
peak. Due to the MR photoautotrophy dependence on their prey, parameters related to CR
have the strongest impact on the MR bloom.

A Model of *Mesodinium Rubrum* Blooms in the Columbia River Estuary

by

Elisabeth J. Sherry

A PROJECT

submitted to

Oregon State University

University Honors College

in partial fulfillment of
the requirements for the
degree of

Honors Baccalaureate of Science in Chemical Engineering
(Honors Scholar)

Presented May 22, 2015
Commencement June 2015

Honors Baccalaureate of Science in Chemical Engineering project of Elisabeth J. Sherry presented on May 22, 2015.

APPROVED:

_____

Yvette H. Spitz, Mentor, representing Earth, Ocean, and Atmospheric Science

_____

Angelicque White, Committee Member, representing Earth, Ocean, and Atmospheric Science

_____

Clara Llebot Lorente, Committee Member, representing Earth, Ocean, and Atmospheric Science

_____

Brandy Cervantes, Committee Member, representing Earth, Ocean, and Atmospheric Science

_____

Toni Doolen, Dean, University Honors College

I understand that my project will become part of the permanent collection of Oregon State University, University Honors College. My signature below authorizes release of my project to any reader upon request.

_____

Elisabeth J. Sherry, Author

ACKNOWLEDGEMENTS

TABLE OF CONTENTS

LIST OF FIGURES

LIST OF TABLES

LIST OF EQUATIONS

1. Introduction

Every year, mixotrophic ciliates create red-water blooms in the Columbia River estuary (Figure 1) between late summer and fall. Studies have concluded that these organisms are either *Mesodinium rubrum/ Myrionecta rubra* (Herfort et al., 2011) or *Mesodinium major* (Garcia-Cuetos et al., 2012; Peterson, personal communication). In this work the organism will be referred to as MR. MR captures and consumes cryptophytes (which will be referred to as CR) that contain phycoerythrin within their chloroplasts (Hansen and Fenchel, 2006), which gives the organisms their red color. The CR that will be the focus of this work are *Teleaulax amphioxeia* (Peterson et al., 2013), common MR prey in the Columbia River estuary. MR consumes the cryptophytes so it can absorb the chloroplasts, nuclei, and mitochondria and use the acquired organs to photosynthesize (Johnson et al., 2007). MR primarily grows by photosynthesis; scientists are uncertain if MR is able to produce its own photosynthetic organs, but they do know that MR absorbs these organs from other organisms (Peterson et al., 2013). This is referred to as "acquired phototrophy" (Hansen et al., 2013). The foreign nuclei help maintain the stolen chloroplasts in the ciliate body. Nevertheless, symbionts appear to degrade over 30 days after grazing (Johnson et al., 2007).

MR are of interest to the scientific community because of the many unanswered questions surrounding their appearance, ecological impact, and ability to remain and grow in a region of short water residence time and low light. Observations collected during two summers in the Columbia River estuary (Herfort et al., 2011) show a

development of MR blooms first in Baker Bay, followed by an established bloom throughout the lower estuary. Scientists currently believe that a decrease in water column

(a)   (b)
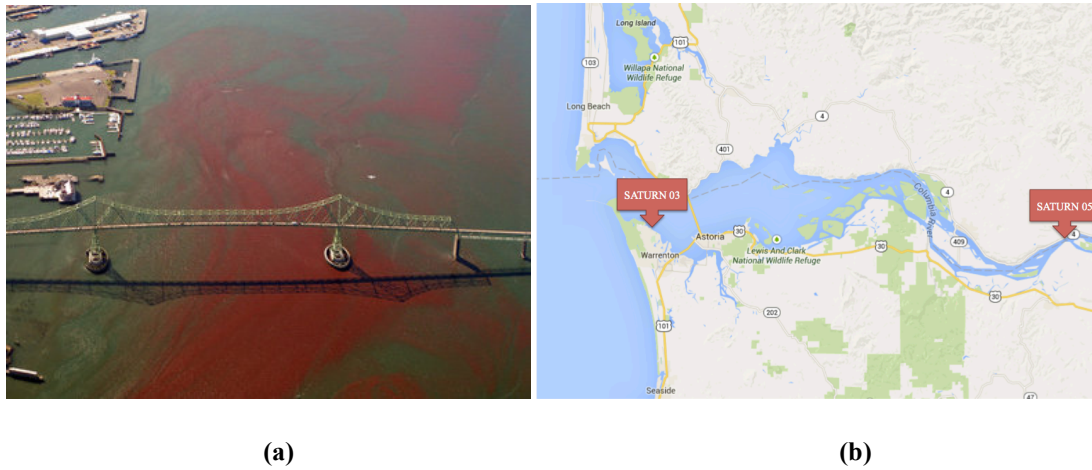
Figure 1: (a) Red MR bloom beneath the Astoria bridge in the Columbia River estuary (photograph taken on September 2008 during ebb tide by Alex Derr). **(b)** Map of the Columbia River estuary with the location of two endurance stations (SATURN 03 and Saturn 05) from the Center for Coastal Margin Observation and Prediction (CMOP).

turbulence encourages the initial appearance of these ciliates in estuaries (Cloern et al., 1991; Crawford et al., 1997). MR can swim up to 1.2 cm s^{-1} and can jump as much as 160 µm in 20 ms (Hansen and Fenchel, 2006), which might allow them to remain in the estuary for months. The mixotrophic cilates tend to remain at the surface of the water during the day to photosynthesize, which is why the red bloom is so visible at the surface of the water. Observations in the Columbia River estuary (Herfort et al., 2011) show a vertical migration influenced by the tides and the light cycle, and it is believed that this

2

behavior is essential to retaining MR in the Columbia River estuary while maximizing solar exposure. It is understood that the blooms dramatically influence the local ecosystem. Global studies have shown MR blooms correspond to increased levels of bacteria, dissolved organic nutrients, oxygen saturation, particulate organic carbon and nitrogen (Wilkerson and Gruneisch, 1990). Specifically in the Columbia River estuary, MR blooms are associated with increased dissolved organic nutrients, increased microbial secondary production, as well as decreased ammonium, nitrate, and dissolved organic carbon levels (Herfort et al., 2011).

A simple biogeochemical model containing the mixotrophic ciliate MR and its cryptophyte prey (CR) is applied in a one-dimensional mode. Model experiments assess the timing of MR bloom formulation, MR retention, and the bloom impact on the Columbia River estuary biogeochemistry. This paper seeks to outline a sensitivity analysis of the model outputs to various model parameters and nutrient fluxes from the ocean and river. Analyses of the model outputs are provided with reference to their biological and ecological significance, more specifically on the concentration and timing of the MR bloom. A MATLAB framework was developed to test the model response to a range of parameters (see the Graphical User Interface, GUI, in Appendix B). This framework may also be used to test the response of MR from other environments such as other estuaries (Crawford et al., 1997) and the Arctic Ocean (Lindholm, 1985), however those possibilities are not explored in this paper.

2. Method

A simple NNPZD is tested in this study to explore (1) the interactions between MR and its prey CR, (2) the effects on the biogeochemistry of the Columbia River estuary, and (3) the reproducibility of population dynamics over multiple years (peaking around August). Figure 2 shows the interactions between the five variables in the ecosystem of a NNPZD model. For the purposes of this study, "phytoplankton" or CR will always refer to the cryptophytes that are prey to MR, and "zooplankton" will always refer to MR.
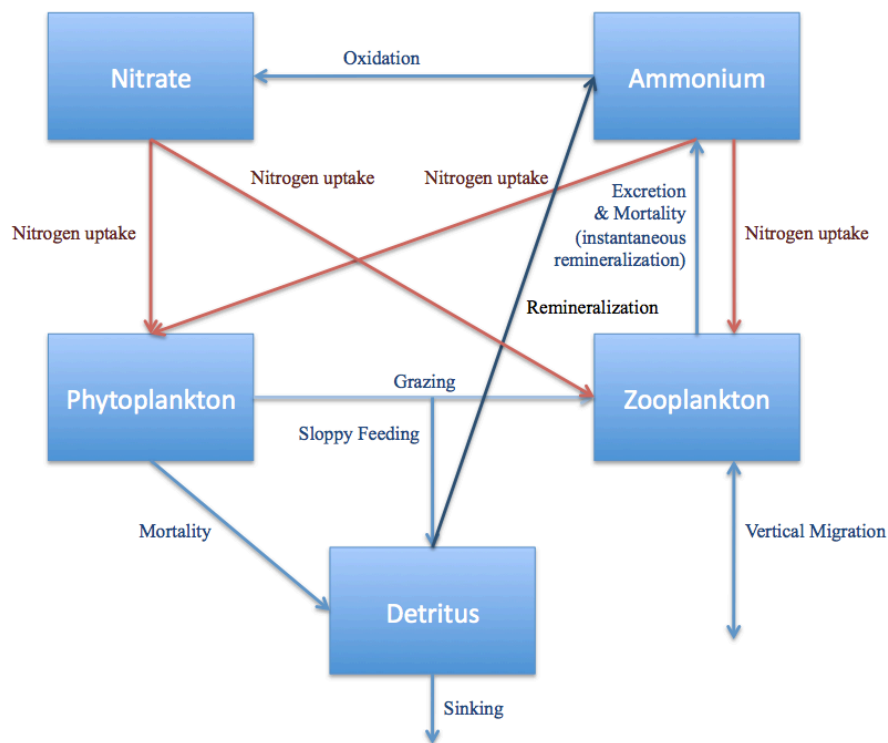
Figure 2: Flow chart depicting the interactions among nitrate, ammonium, phytoplankton, zooplankton, and detritus. The term "phytoplankton" will be used to refer to the CR and "zooplankton" will be used to refer to MR in this paper. The red arrows are related to the process of photosynthesis.

Mathematical representations of time evolution of the five component ecosystem model are given in Equations 1 – 6. They are based on the Spitz et al. (2005) model and have been modified in Spitz et al. (2015). The five components are phytoplankton (CR), zooplankton (MR), nitrate (NO_3), ammonium (NH_4), and detritus (D).

$$\frac{\partial CR}{\partial t} = -Ivlev \times MR + (uptakeNO_3 + uptakeNH_4) \times lightlim \times templim \times CR \qquad (1)$$
$$- mp \times CR$$

$$\frac{\partial MR}{\partial t} = (uptakeNO_3 + uptakeNH_4) \times lightlim \times templim \times photopop \times MR \qquad (2)$$
$$+ Ivlev \times \gamma \times MR - mz \times MR + swim(t)$$

$$\frac{\partial NO_3}{\partial t} = -uptakeNO_3 \times lightlim \times templim \times CR - uptakeNO_3 \times lightlim \times templim \qquad (3)$$
$$\times photopop \times MR + \Omega \times NH_4 + AdvecNO_3$$

$$\frac{\partial NH_4}{\partial t} = -uptakeNH_4 \times lightlim \times templim \times CR - uptakeNH_4 \times lightlim \qquad (4)$$
$$\times templim \times photopop \times MR + mz \times MR - \Omega \times NH_4 + rem \times D$$

$$\frac{\partial D}{\partial t} = (1 - \gamma) \times Ivlev \times MR + mp \times CR - rem \times D + sinking \qquad (5)$$

Model parameters are given in Table 1. The functions *uptake, Ivlev, lightlim, templim* and *AdvecNO₃* are defined in Appendix A. Vertical migration, denoted as *swim(t)* in Equations 2, is defined to mimic the vertical MR displacement in response to the ebb and flood tides in the estuary and observed in the phycoerythrin field measured at the north channel endurance station SATURN 01.

Table 1: Optimal parameter values determined through sensitivity analysis.

Parameter	Symbol	Value
Time interval (d)	dt	0.0104
Phytoplankton maximum uptake rate (d^{-1})	V_M	1
Zooplankton maximum uptake rate (d^{-1})	Z_M	1.37
Half saturation for phytoplankton NO3 / NH4 uptake (mmol Nm^{-3})	ks	1.5 *
Light attenuation by zooplankton (m^{-1})	kz	0
Light attenuation by phytoplankton (m^{-1})	kp	0.0095 *
Light attenuation by pure water (m^{-1})	kw	0.26
Phytoplankton mortality rate (d^{-1})	mp	0.33
Zooplankton maximum grazing rate (d^{-1})	rm	1.5
Ivlev constant (mmol Nm^{-3})$^{-1}$	λ	0.05 *
Growth efficiency for zooplankton	γ	0.55
Zooplankton excretion/mortality rate (d^{-1})	mz	0.145
Initial slope of P-I curve ((Wm^{-2})$^{-1}$d^{-1})	α	0.10 *
NH4 oxidation rate (d^{-1})	Ω	0.25 *
Detritus remineralization rate (d^{-1})	rem	0.30
Maximum vertical swimming rate (mm s^{-1})	$swim_{max}$	0
Detritus sinking rate (d^{-1})	$wdet$	-3.56
Phytoplankton sinking rate (m d^{-1})	$wphy$	0
CR:MR maximum photosynthesis cell ratio	$r(Cr, MR)$	10

* (Spitz et al., 2005)

The *swim(t)* function (Equation 6 and Figure 3) as defined in this study is based on the results from a particle tracking simulation in the estuary (Spitz, 2011) and follows the M2 tidal cycle with an upward (downward) movement during ebb (flood). The phase of the M2 tide at SATURN 01 is 298˚. Optimal retention was achieved in the particle tracking simulation for ΔT equal to 2.8 hours.

$$swim(t) = swim_{max} \times \cos\left[2\pi\left(\frac{t+\Delta T}{12.42} + \frac{\Phi}{360}\right)\right] \tag{6}$$

where *t* and *ΔT* are in hours, Φ is the phase in degrees and *swim$_{max}$* is defined in Table 1.
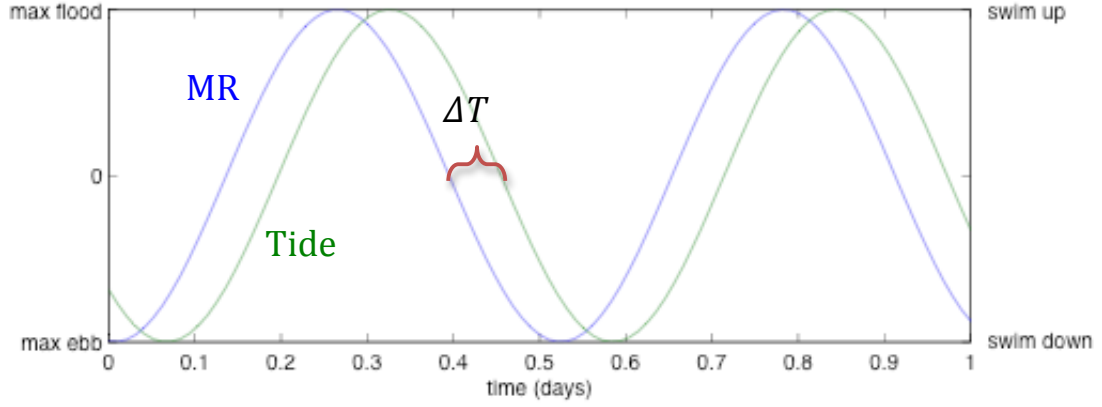
Figure 3: Plot of *swim(t)* (**MR**) and tidal frequency (**Tide**) over one day. The variable ΔT is the number of hours that the MR should swim ahead of the tide, and was optimized to 2.8 hours (Spitz, 2011).

Photopop is a function that represents growth adjustment based on the number of CR that MR acquires for photosynthesis, with symbiont deterioration over a 30-day period (Johnson et al., 2007). The function is given in Equation 7 and is illustrated in Figure 4.

$$\text{if } t \leq 30 \text{ then} \quad photopop(t) = \sum_{j=1}^{t} graz(j) \tag{7}$$

$$\text{if } t > 30, \text{ then} \quad photopop(t) = \sum_{i}^{30} \tanh\left(\frac{i}{6}\right) graz(t - i)$$

where t is time in days and graz is the grazing function defined in Appendix A. Photopop is limited by an upper value corresponding to a maximum of CR that MR can acquire for photosynthesis (see discussion in subsection 3.5).
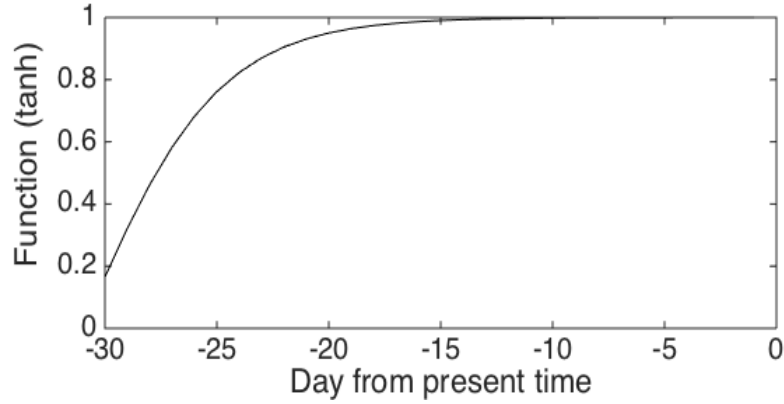
Figure 4: Function of Equation 7 that represents degradation of the symbiont over a 30 day period.

Nitrate advection (Equation 14 in Appendix A) is calculated using ocean and river fluxes from the SELFE circulation model outputs for 2010 (Zhang and Baptista, 2008) and concentrations recorded in 2010 at SATURN 05 (river side) and SATURN 03 (ocean side) (Figure 1). Time evolution of the surface nitrate concentration at SATURN 03 and 05 are displayed in Figure 5. In the considered simulations, the water column experiences spatially constant fluxes into and out of the estuary from the ocean and river.

MR and CR are also capable of being advected and the same function as for nitrate is defined in that case. These advection terms were not fully calibrated, however, so throughout this work *AdvecMR* and *AdvecCR* are set equal to zero.
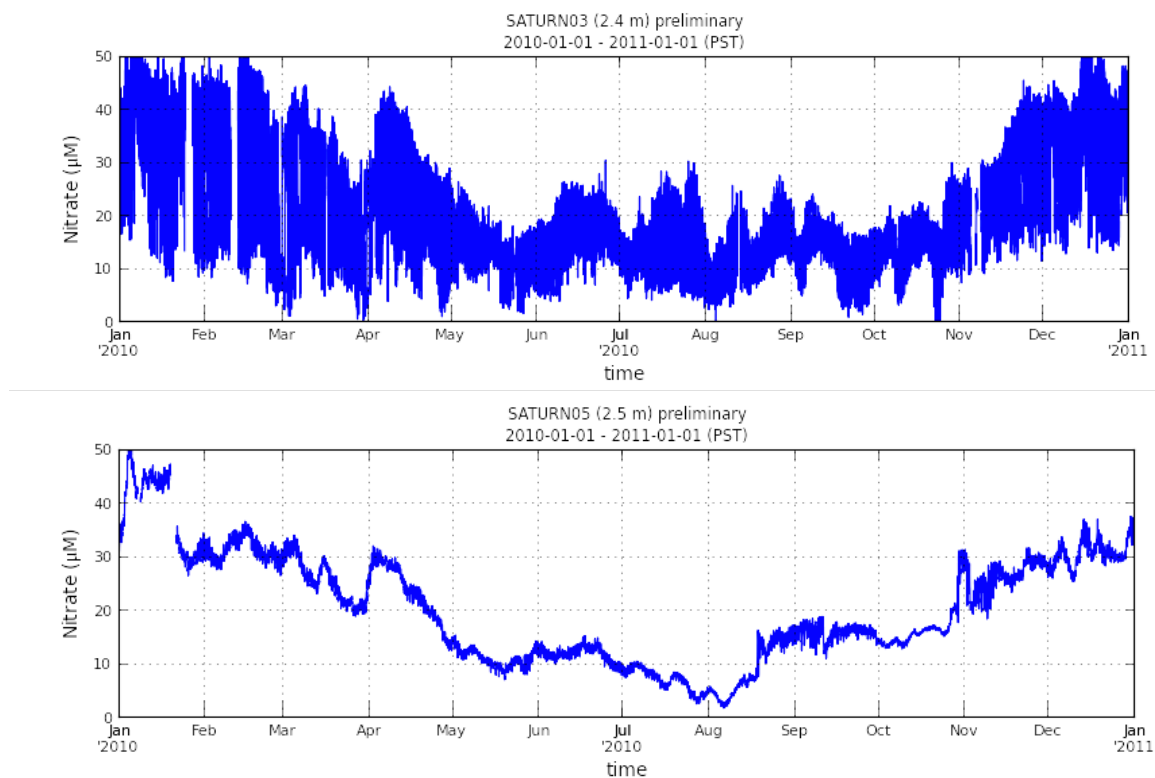
Figure 5: Nitrate concentration at SATURN 03 and SATURN 05 in 2010, used to simulate nitrate advection.

The model is run in a one-dimensional (vertical) framework with vertical migration of MR, advection of nitrate, and sinking of detritus. The vertical domain has a total depth of 21 meters with a one-meter resolution and the time step used to solve the equations is 15 minutes.

The impacts of nitrate advection, in addition to other Table 1 parameters that produced significant model responses in the sensitivity analysis, are explored in section 3. Significant changes to MR bloom timing, growth, and retention are the focus of the analysis.

9

3. Results and Discussion

Nitrate advection, MR and CR maximum uptake rates, MR and CR mortality rates, MR photosynthesis rate, minimum concentrations before the bloom, and vertical migration were tested in the sensitivity analysis with results shown, in that order, below. This section first describes an "optimal simulation" setup and results in the subsection 3.1. The following subsections (3.2 - 3.7) discuss the results of each sensitivity analysis with respect to the optimal simulation.

3.1 Optimal Simulation

The objective of this project was to design a simple model that would produce an MR bloom with timing, growth, and duration that mimicked observed bloom patterns in the Columbia River estuary. Phycoerythrin and chlorophyll measurements at SATURN 03 during late summer – early fall 2010 serve as reference for the model simulation of the MR bloom in the Columbia River estuary (Figure 6). It should be noted that these time series reflect blooms of both MR and CR, as both contain phycoerythrin and chlorophyll.

As shown in Figure 6, chlorophyll begins to increase on August 15th, values remain elevated through most of September, and then peak again around October 5th. Maximum chlorophyll concentration is measured during two periods, around September 5th and in early October. The phycoerythrin at SATURN 03 follows a very similar temporal pattern. The high frequency fluctuations in the data are due to daily/tidal cycles of migration and

horizontal transport effects that are not included in the simple one-dimensional model set-up.
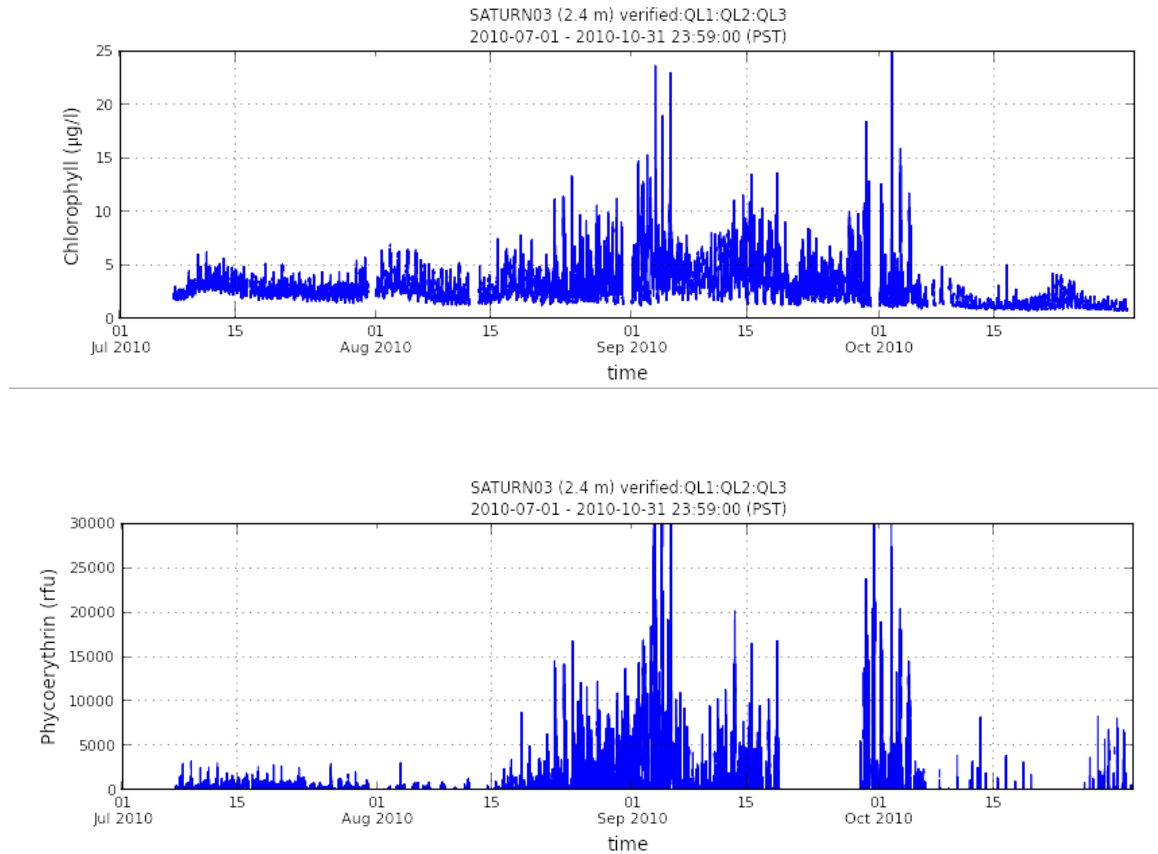
Figure 6: (Top) Measured chlorophyll concentrations in (μg/l) from July 1, 2010 to October 31, 2010. **(**Bottom) Measured phycoerythrin in (rfu) from July 1, 2010 to October 31, 2010.

Nutrient and biomass concentrations illustrated in Figure 7 match observed trends seen in the Columbia River estuary (Figure 6), and can be modeled over multiple years. The optimized simulation parameter values that produced Figure 7 are listed in Table 1. Note the optimal simulation does not include vertical migration or cell advection but does include nitrate advection.
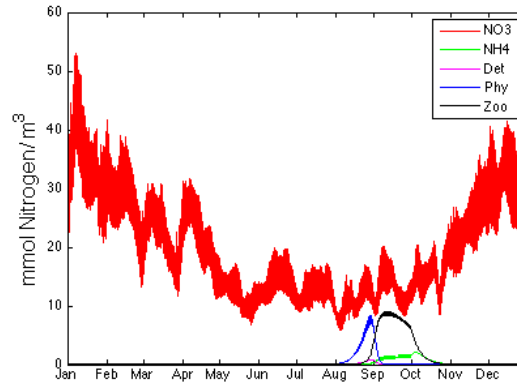
Figure 7: Optimal simulation of the surface MR, CR, nitrate, ammonium and detritus concentration for one year. The model was run with nitrate advection and without vertical migration or cell advection. Parameters used for this simulation are listed in Table 1.

Figure 8 illustrates the combined surface blooms of MR and CR in the estuary. The bloom begins in August, reaches its maximum value in early September, and sharply declines in October. The high frequency fluctuations seen in this simulated time series are due to the daily light cycle.
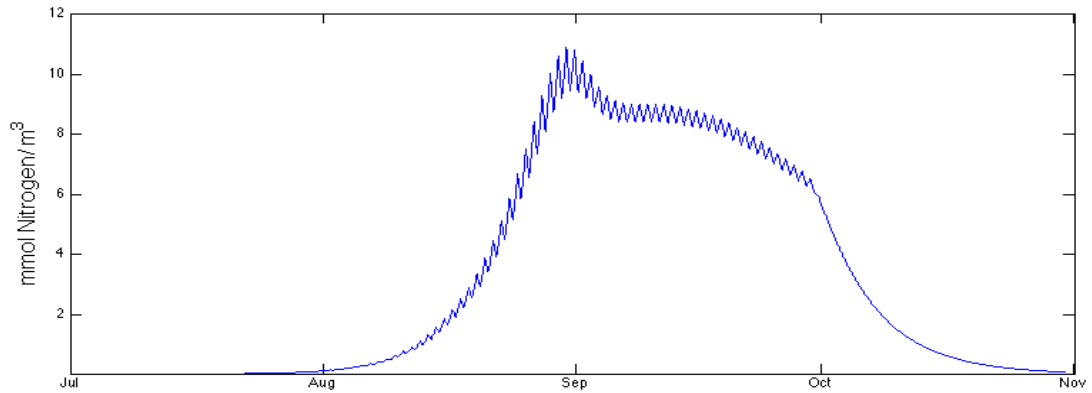
Figure 8: Modeled MR and CR bloom from August to November with imported nitrate data from 2010 at 2.4 m depth, without MR or CR advection and without vertical migration. Maximum bloom approaches 11 mmol N m^{-3}.

Chlorophyll (Chl) concentrations as high as 20 µg/l have been observed at the surface of the Columbia River estuary (Sullivan et al. 2001; CMOP SATURN 03, 2010). Modeled chlorophyll can be obtained from modeled MR biomass using a Chl:N ratio of 2.1 ± 0.5 mg Chl mmol N^{-1} (Johnson et al., 2006), This ratio is very similar to what has been observed for diatoms off the Oregon coast. Dickson (1994) and Dickson and Wheeler (1995) obtained a Chl:N ratio of 2.19 ± 0.45 mg Chl mmol N^{-1} from a station 8 km offshore of Newport from July 1990 to August 1991. Using the 2.1 mg Chl mmol N^{-1} value for Chl:N, the simulation demonstrates a maximum of 23 mg Chl m^{-3}, which is in the range of Chl observed at SATURN 03.

Detritus, ammonium, and CR concentrations at the surface have observable responses to the MR bloom in this simulation. The most obvious relationship is between MR and CR; once temperature, light, and nutrient conditions in the estuary are favorable, phytoplankton begin to bloom and MR are able to graze. MR grazing depletes the CR population faster than the natural mortality rate and exceeds the CR growth rate in September. Additionally, detritus concentration increases and peaks from mid-August to early September as MR begins to graze the abundant phytoplankton. "Sloppy feeding" is one source of detritus; as MR grazes, some of the organic material does not get ingested and is lost to detritus. The other source of detritus is CR mortality, imposed by the CR mortality rate parameter. The mortality rates are imposed as a percentage of the total population. Therefore, as biomass concentration in the bloom increases, mortality also increases. The MR bloom also triggers increased ammonium concentrations. Ammonium is the product of excretion and instantaneous remineralization (MR mortality). Its

maximum concentration does not exceed 3 mmol N m^{-3}, and its peak coincides with the beginning of the sharp bloom decline. Concentrations between 1 mmol N m^{-3} and 3 mmol N m^{-3} have been observed in the main channel red water (Herfort et al., 2012).

There does not appear to be a significant depletion of nitrate in response to increasing MR or CR. In the one-dimensional model, the nitrate lost to nitrogen uptake processes is negligible compared to the input by advection from the ocean and river. A three-dimensional model would show the impact of the bloom on nitrate concentration in greater detail because spatial changes in estuary fluxes are included.
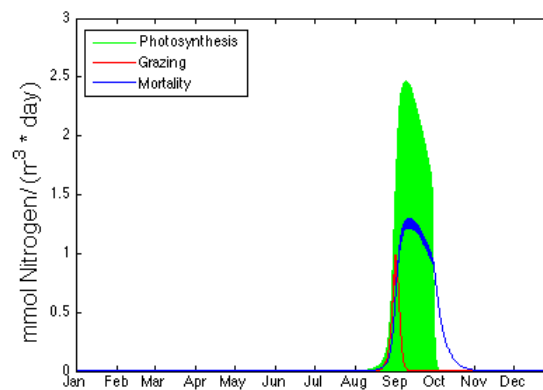
Figure 9: Photosynthetic growth, grazing, and mortality rates (plotted as absolute value for comparison) of MR at the surface.

In the optimal simulation, there is initially a balance between the three biological forcing mechanisms, which leads to the MR bloom (photosynthetic growth, grazing, and mortality). Photosynthetic growth becomes larger than the grazing contribution to MR growth in early September when grazing begins to decline. By mid-September the rate of

growth of the bloom slows down and approaches its peak due to a balance between photosynthetic growth and mortality of MR. MR has stopped grazing and growth related to photosynthesis begins to decline as the organs required to photosynthesize deteriorate without being replaced. At the beginning of October, the mortality rate exceeds the growth rate and the population makes a sharp decline (controlled by the mortality rate) that ends in November. Figure 9 illustrates that photosynthesis contributes significantly more to the MR bloom than grazing, but once grazing has finished the process is unable to sustain itself and the bloom ends.

3.2 Nitrate Advection

Adding a real flux of nitrate in the model regulates the amount of nitrogen in the system. Without these fluxes, it would be difficult to reproduce a realistic bloom over multiple years. Figure 10 shows the optimal model behavior over 3 years, and the impact of including nitrate advection calculated from observations on the model outputs for the same 3-year period.

Figure 10a represents an approximation of the biogeochemical response when a continuous nitrate source from the river takes the form of a hyperbolic tangent function (Figure 10b). The curve imposes 20% maximum inlet river flows carrying nitrate in the winter, has a steep increase of 10% per month from March to May, a steep decrease of 10% from August to October, and peak in the middle of June. A constant nitrate concentration input is applied to these flows, providing about 40 mmol N m^{-3} from
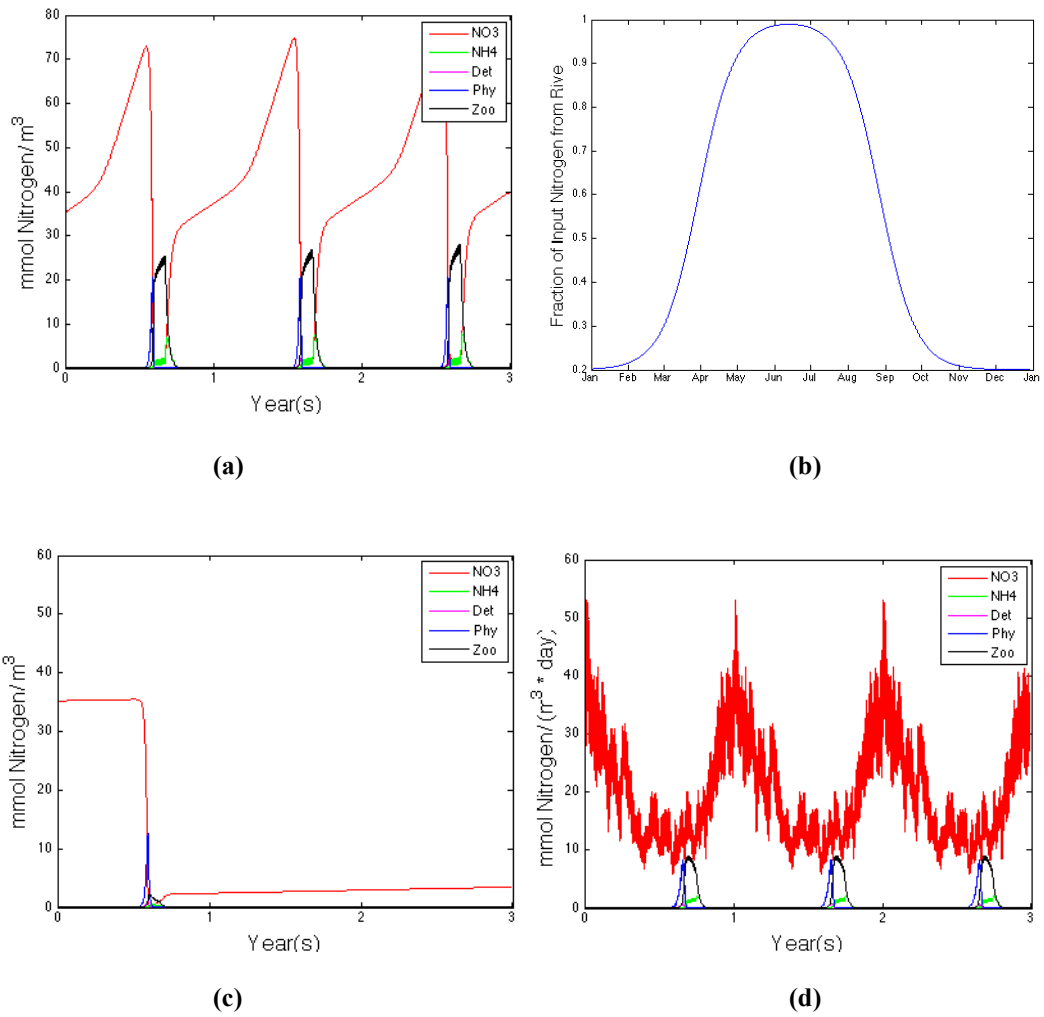
Figure 10: (a) A three-year run with approximated nitrate source based on **(b)** a hyperbolic tangent function controlling the percent maximum nitrate source from the river over the year. **(c)** A three-year run of the basic case without nitrate advection. **(d)** Optimal simulation: a three-year run with nitrate advection. Note that the scales differ between different model runs.

January to June. The function is based upon Columbia river flow trends (U.S. Bureau of Reclamation, U.S. Army Corp of Engineers, and Bonneville Power Administration, 2001); however, it does not account for water entering/exiting the ocean, nor is it a

16

substitute for measured data, especially since a reasonable constant nitrate concentration range that can be applied to this approximation is uncertain. Figure 5 illustrates the dynamic seasonal change in nitrate concentration measured from the river and ocean over the course of one year.

In Figure 10d, the nitrate concentrations from Figure 5 are applied to an advection term to simulate realistic fluctuations in nitrate concentration in the estuary. Annual nitrate advection patterns lead to a realistic bloom of MR and CR in the late summer and fall (Figure 10d) while MR and CR are unable to bloom multiple years without an external source of nutrients (Figure 10c). With nitrate advection in the optimal simulation (Figure 10d), the imposed nitrate concentration exceeds the model requirements to sustain a bloom, which leads to model results that are comparable to observed trends in the Columbia River estuary. The model is also more stable in the presence of slight parameter deviations from Table 1 values due to the abundance of nitrate.

3.3 Maximum Uptake Rate

Based on the literature surveyed during this study, it appears that there is a large uncertainty on the maximum nutrient uptake rate of MR, and the question of whether MR and CR have the same maximum nutrient uptake rate is still open (Peterson et al., 2012 & 2013). Nutrient uptake is a necessary component to MR and CR growth during photosynthesis. Equations 1 and 2 include NO_3 and NH_4 uptake in the calculation of photosynthetic growth for MR and CR, and the uptake terms are calculated with the

Michaelis-Menten formulation (see Equation 10 in Appendix A). The model was designed to accommodate unequal maximum uptake rates in MR and CR so that scenarios with equal and unequal uptake rates could be tested. A sensitivity analysis is explored in Figure 11.

(a)

(b)
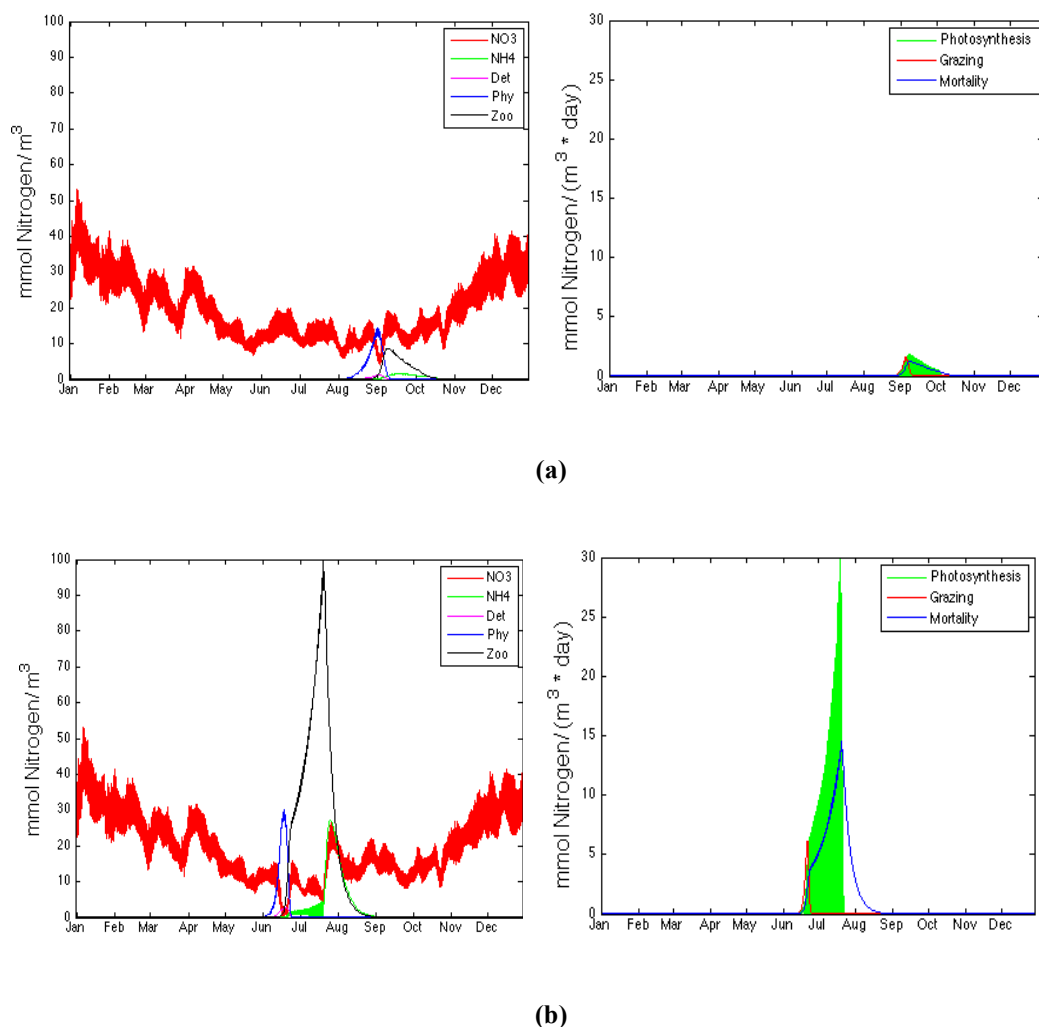
Figure 11: (Left) Surface concentrations over one year and (right) MR photosynthesis, grazing and mortality for the following simulations: **(a)** $V_M = Z_M = 1.00$ d^{-1}, and **(b)** $V_M = Z_M = 1.37$ d^{-1}.

(c)
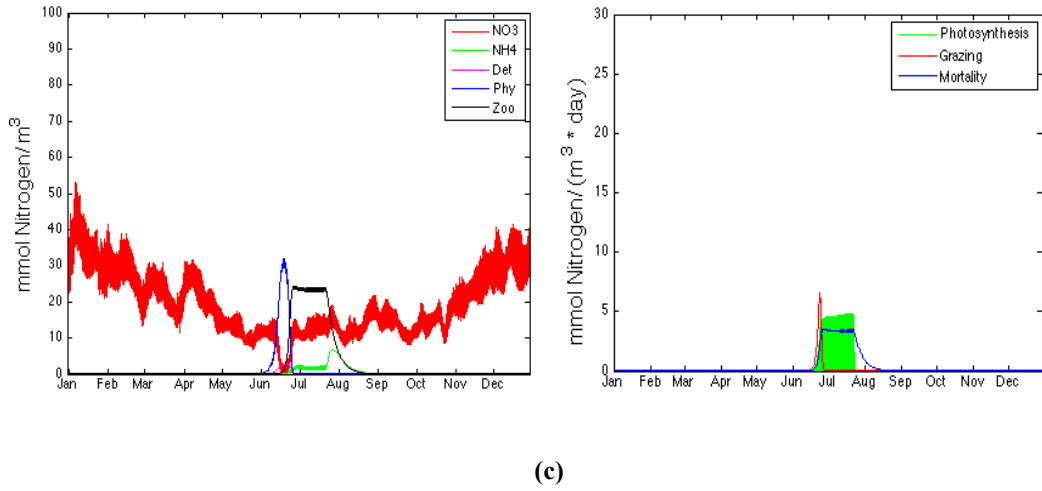
Figure 11 (continued): (Left) Surface concentrations over one year and (right) MR photosynthesis, grazing and mortality for the following simulations: **(c)** V_M = 1.37 and Z_M = 1.00 d^{-1}. V_M is the CR uptake rate and Z_M is the MR uptake rate. Note that the scales vary between the different model runs and between the left and right plots within each model run. In the optimal simulation, V_M = 1.00 d^{-1} and Z_M = 1.37 d^{-1}.

The model is highly sensitive to a change in CR maximum uptake rate. A 0.37 d^{-1} increase in the CR (Figures 11b-c) maximum uptake rate results in CR blooms occurring two months earlier, with a maximum nearly three times the value from the optimal simulation (Figure 7). The MR bloom lasts twice as long and achieves a maximum that is approximately 10 times higher than in the optimal simulation in Figure 11b. When the MR uptake rate is concurrently decreased by the same amount, the MR bloom reaches about twice its optimal simulation maximum. In both cases, the beginning of the MR bloom still occurs half a month after the beginning of the CR bloom and length of the CR bloom is reduced by a few days compared to the optimal run. A 0.37 d^{-1} decrease of MR uptake rate while keeping the CR uptake rate from the optimal simulation does not show large changes in either timing or magnitude of the CR and MR bloom (Figure 11 a).

When MR uptake rate is higher than CR uptake rate, photosynthetic growth reaches values that are larger than growth due to grazing. However, in all cases the bloom is sustained primarily due to photosynthetic growth, which means MR depends most heavily on the organs it acquired from its prey to sustain the bloom. Although photosynthesis is still the dominant factor in MR growth during the bloom, the mortality rate matches the photosynthetic growth curve more closely in both Figures 11a and 11b than in the optimal simulation (Figures 8 and 9). When CR nitrogen uptake rate is higher than MR nitrogen uptake rate (Figure 11c), photosynthetic growth and mortality are tightly coupled and remain mostly constant from late June to late July,

The results of this sensitivity analysis indicate that the MR bloom is more sensitive to changes in CR maximum uptake rate than MR maximum uptake rate. This is most likely because MR depends on grazing to begin the bloom. The optimal simulation rejects the assumption that MR has the same maximum uptake rate as its prey, therefore independent uptake rates for MR and CR lead to the model emulating more realistic biology. However, Figure 11a shows that plausible surface blooms can be achieved in the first year with equal maximum uptake rates. Results indicate that the range of rate values is tightly constrained, i.e. MR blooms are highly sensitive to changes in the maximum uptake rates. This results in optimum uptake rates that must be fine tuned ($V_M = 1.00$ d^{-1} and $Z_M = 1.37$ d^{-1}) to produce blooms comparable to chlorophyll-a and phycoerythrin measurements at SATURN 03 in 2010. Laboratory experiments will be necessary to constrain these values better.

3.4 Mortality Rate

The mortality rate of MR has a direct impact on the slope of population decline at the end of an MR bloom. CR mortality rate indirectly affects the timing and magnitude of the MR bloom through grazing. These parameters are imposed as a percent mortality of the entire population (refer to Equations 1 and 2) of their respective species. Figure 12 explores simulation sensitivity to changes in planktonic mortality rates.

(a)

(b)

(c)
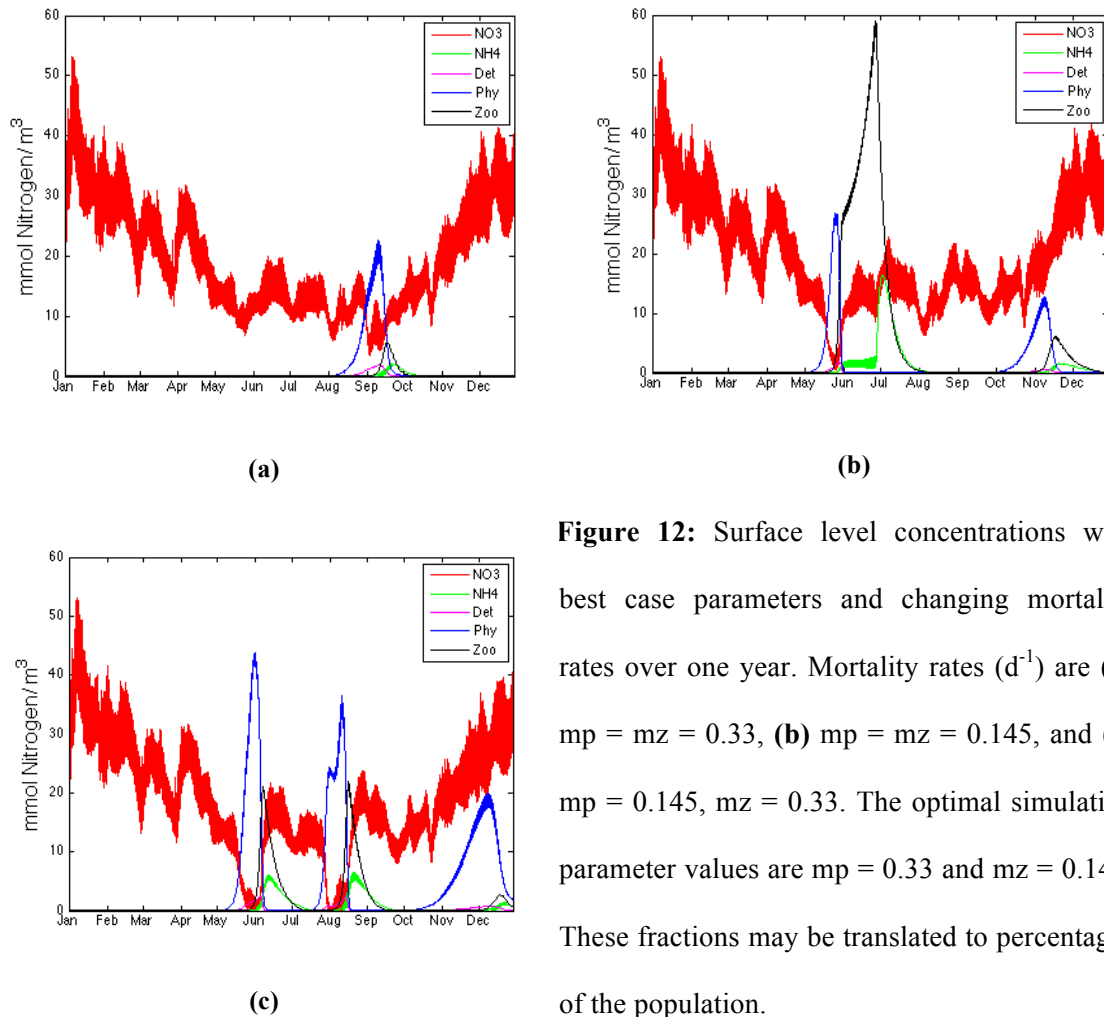
Figure 12: Surface level concentrations with best case parameters and changing mortality rates over one year. Mortality rates (d⁻¹) are **(a)** mp = mz = 0.33, **(b)** mp = mz = 0.145, and **(c)** mp = 0.145, mz = 0.33. The optimal simulation parameter values are mp = 0.33 and mz = 0.145. These fractions may be translated to percentages of the population.

21

The elevated CR mortality rate in Figure 12a and the optimal simulation causes the MR to bloom once a year in September. When the CR mortality rate is reduced from 33% mortality to 14.5%, MR initially bloom in the month of June, with the potential to bloom once or twice more in the same year given prey and nutrients are abundant. Figures 12b and 12c demonstrate a 66% decrease in the first bloom's maximum concentration when the CR mortality rate remains at 14.5% and the MR mortality rate increases from 14.5% to 33%. A similar difference (approximately 50%) in the initial bloom peak concentrations occurs when the MR mortality rate increases compared to the optimal simulation (Figures 7 and 12a).

The frequency of MR blooms in a year depends on both MR and CR mortality rates, because timing is strongly influenced by prey concentration. This makes it difficult to compare second and third blooms in a year between different runs. The MR mortality rate has a direct impact on the magnitude of the bloom; however, because MR depend on grazing to start a bloom, the mortality rate of MR does not directly correlate with the timing or frequency of blooms in a given year. Timing of the first bloom can instead be inversely correlated with the CR mortality rate. A higher CR mortality rate will delay both the CR and MR blooms by removing CR cells rapidly, reducing the remaining number of reproductive cells, and reducing the MR cell initial source of growth. An elevated MR mortality rate will reduce the total MR population, but it will not impact the rates of grazing and photosynthesis per unit MR. Once mortality begins to outcompete grazing and photosynthesis, the population declines at a rate that is proportional to the mortality. Higher MR mortality rates allow more CR to grow since the total number of

22

grazed prey cells is reduced. This, in conjunction with a reduced CR mortality rate, can trigger one or two additional CR and MR blooms in one year.

3.5 Rate of Photosynthesis

Plots of photosynthesis, grazing and mortality rates for MR illustrate the role each plays in the shape of an MR bloom. Grazing instigates the bloom, determines when the bloom starts and facilitates a rapid climb in MR concentration. The bloom maximum often occurs at the end of the grazing period or shortly after photosynthesis becomes the driving force for growth. Photosynthesis sustains the bloom. Then the mortality rate controls the peak of the bloom and shapes the decline. Mortality in conjunction with photosynthesis determines when the end of the bloom occurs. Grazing and mortality rate have been discussed at length in earlier parts of this analysis. This section will explore the sensitivity of MR bloom characteristics to photosynthesis, specifically by manipulating the maximum CR to MR cell ratios involved in MR photosynthesis.

As mentioned in section 2, *photopop* is a function that imitates the limitation of growth based on the number of CR grazed with symbiont deterioration over a 30 day period. From the moment they are absorbed, symbionts deliver diminishing returns over time, with total degradation (no effect on growth) of the given symbiont after day 30 (refer to Equation 7). An additional limitation is imposed by Equation 8 to control the maximum amount of CR that may be absorbed by MR at a given point in time. If the number of CR per MR cell is greater than a given value *maxthMR*, then MR does not acquire more CR

for photosynthesis but still continues to graze. This is mathematically imposed in the model when the lower *maxthMR* value replaces the higher *photopop* value that is calculated from grazing.

$$maxt\,hMR = a\,r(CR, MR) \tag{8}$$

where *a* is the ratio of nitrogen content in CR and MR cells and r(*CR,MR*) represents the number of CR cell per MR cell.

Since our model is in terms of nitrogen and the nitrogen content of CR and MR cells are largely different, it is imperative to take into account this difference. For this study we considered 669 pg C cell^{-1} and a C:N ratio of 5 mmol C:mmol N for *Mesodinium* and 29 pg C cell^{-1} and a C:N of 5 mmol C:mmol N for cryptophyte (Johnson and Stoeker, 2005; Johnson et al., 2006). The value of r(*CR,MR*) is set to 10 in the optimal simulation based on literature review (Yih et al., 2004). Both *photopop* and its upper limit *maxthMR* play a significant role in MR photosynthesis rate, the first term in the zooplankton component calculation (Equation 2).

The sensitivity analysis in Figure 13 focuses specifically on the relationship between the variable r(*CR,MR*) in the *maxthMR* calculation and the dynamics of the MR bloom. A change of r(*CR,MR*) from 1 to 10 triggers an earlier bloom by a few days and a slight increase in the MR bloom maximum. It is interesting to note that a single CR cell is capable of triggering a MR bloom that is comparable to the result of 10 CR cells, given

sufficient nutrients. This supports the notion that MR is capable of sustaining a bloom even after grazing only a single CR cell. The change of r(*CR,MR*) from 10 to 20 is far more significant. The peak of the MR bloom appears to respond non-linearly to an elevated absorption limit, but there is a clear correlation between the absorption limit and the peak of the MR bloom because absorption facilitates photosynthetic growth. A less drastic change in the timing and length of MR bloom occurs in response to a change from 1 to 20 in the CR absorption maximum. However, as r(*CR,MR*) increases, the bloom starts earlier in the year, peaks earlier, and lasts longer. The change of r(*CR,MR*) from 1 to 20 doubles the length of the MR bloom from less than one month in September to approximately two months from mid-August to mid-October.

There is also a marked decrease in CR population as the absorption limit increases (primarily compared between Figures 13b and 13a). The beginning of the CR bloom is unaffected by any change in absorption limit, so it begins in August in every run of this sensitivity analysis. However, as r(*CR,MR*) increases, the CR peak occurs sooner, achieves a lower concentration, and declines sooner because there are more grazers.

If the limit of CR absorption by MR is increased, MR is able to absorb more symbionts through grazing and therefore grow more MR through photosynthesis. The elevated MR then translates to a larger population that can graze CR. More CR are grazed, then absorbed, and converted to MR growth. This cycle perpetuates until the CR population is lost to grazing.
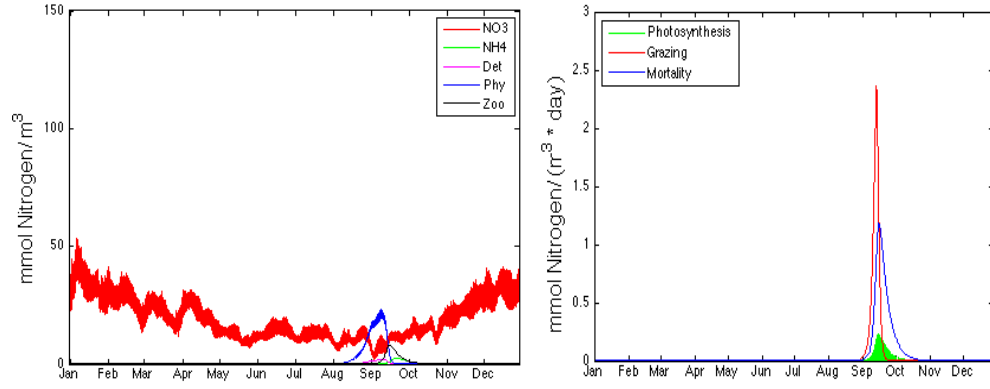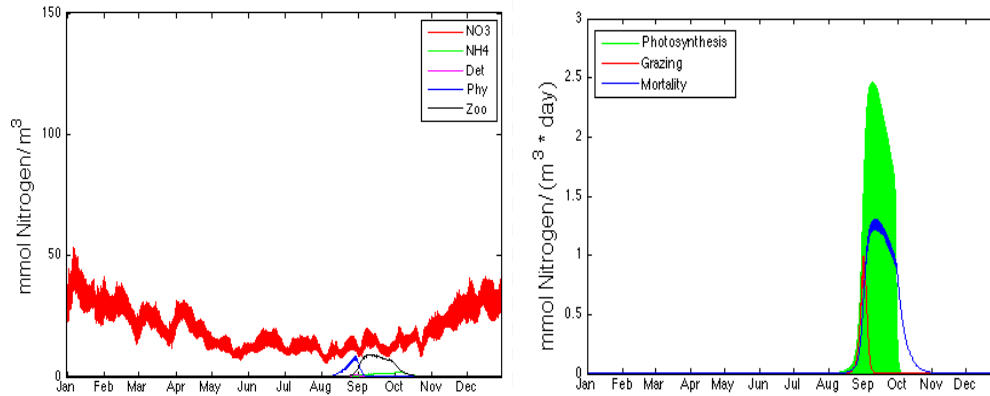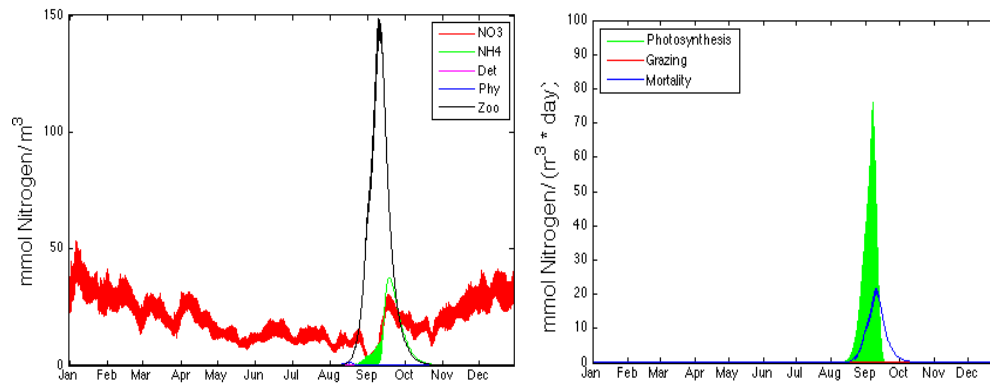
Figure 13: (Left) Surface concentrations over one year with optimal simulation parameters and (right) MR photosynthesis, grazing and mortality with the maximum CR:MR cell ratios for MR photosynthesis: **(a)** 1, **(b)** 10 (optimal simulation), and **(c)** 20. Note the different scales between the figures.

The model currently includes perpetual MR grazing, independent of absorption limits and photosynthesis. It is known that in species like *Karlodinium*, photosynthesis is supplemented with feeding on cryptophytes (Adolf et al., 2006); however it is unknown whether MR mirrors this behavior. Further sensitivity analysis should be conducted with the grazing turned off during photosynthesis to isolate the effects of each process on the MR bloom. As an initial prediction, one may expect to see a small or negligible decrease in the peak of the MR bloom, but a longer bloom time (with the same start date) or increased propensity for multiple blooms due to higher concentrations of available prey when the MR cells are not photosynthesizing. Photosynthesis drives the growth rate to its peak while grazing extends the length of the bloom.

3.6 Seed Concentrations

Initial seed concentrations for the five major components of this model – MR, phytoplankton, nitrate, ammonium, and detritus – were chosen to work in conjunction with the nitrate advection to produce a symmetrical yearly biogeochemistry cycle. A minimum seed concentration of 0.01 mmol N m^{-3} is also imposed on MR to prevent extinction in the estuary. Table 2 lists the initial seed concentrations for each component:

Table 2: Component seed concentrations and minimum concentrations.

Initial Seed Concentration [mmol N/ m^3]				
MR	**CR**	**NO$_3$**	**NH$_4$**	**Detritus**
0.01	1×10^{-10}	35.21	0.0046	1×10^{-10}

Over several years, the initial seed concentration has a noticeable impact on bloom patterns and MR minimum concentration has a significant impact on the initialization of a bloom. The model sensitivity is most visible below the estuary surface. An analysis on the impact of initial concentrations over three years is explored in Figure 14.

(a) (b)

(c) (d)
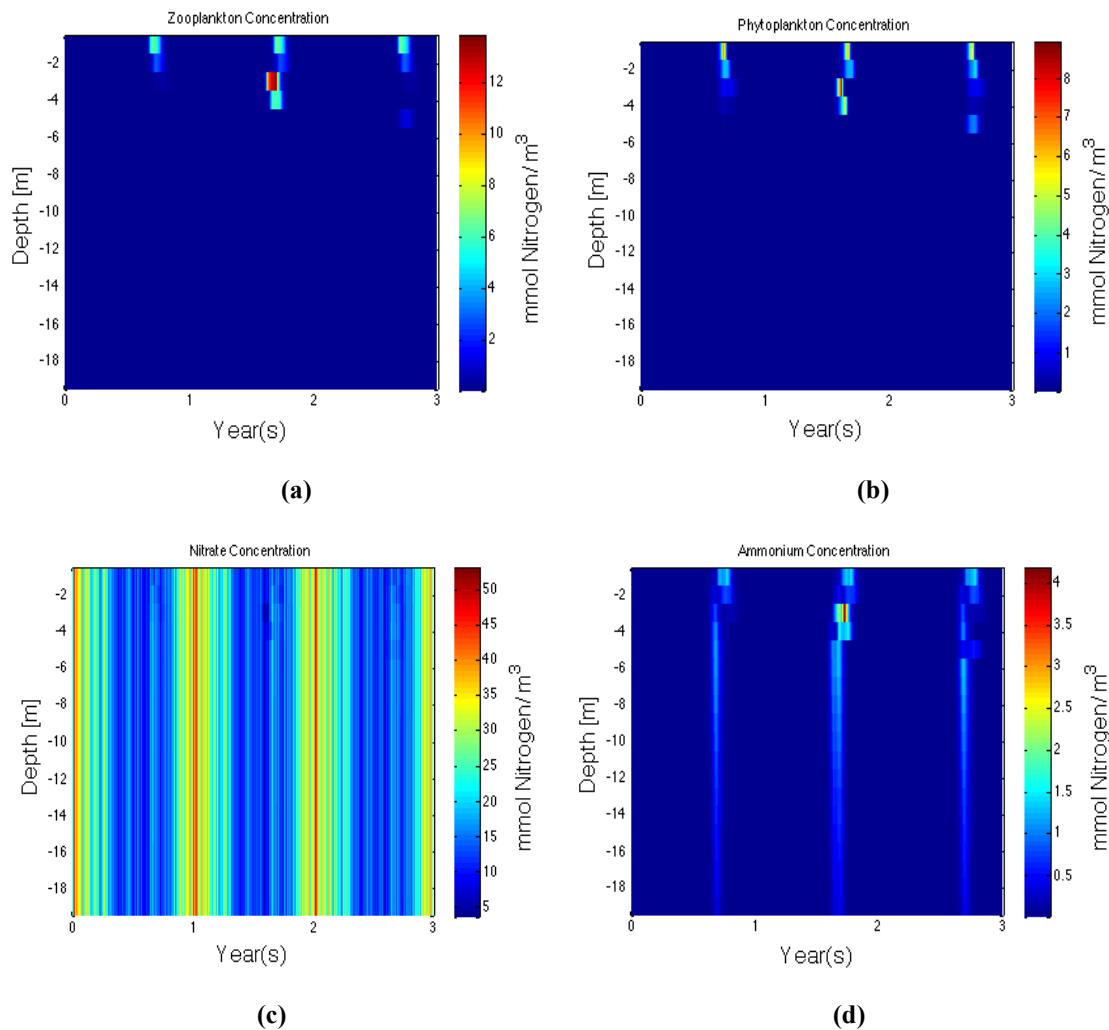
Figure 14: Nutrient and biological concentrations through the water column over time. The five components are as follows: **(a)** MR, **(b)** CR, **(c)** nitrate, **(d)** ammonium,

Detritus Concentration

Depth [m]

Year(s)

mmol Nitrogen/ m³
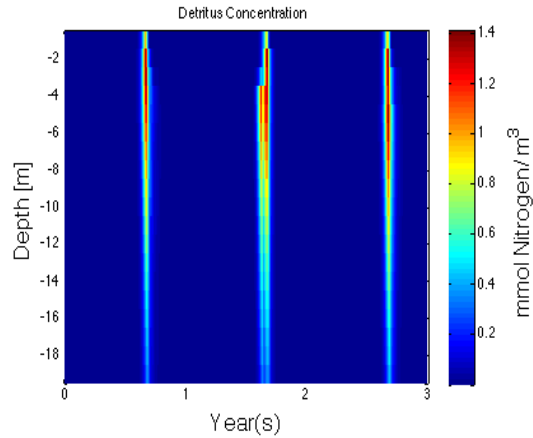
(e)

Figure 14 (continued): (e) detritus.

The surface level concentrations appear to be symmetrical in timing and magnitude every year over a three-year period (Figures 10c and 14). This result validates the inclusion of nitrate advection in the model; however, with the current initial conditions and imposed minimum concentrations, Figure 14 demonstrates that the yearly pattern does not hold constant through the water column.

Annual bloom similarity is most strongly affected by the seed concentrations. The initial concentrations listed in Table 2 were sufficient to produce nearly identical bloom patterns at the surface with the addition of nitrate advection. However, optimization to produce identical yearly blooms throughout the water column is ongoing. A run simulating several years will approach an asymptote of similarity, beginning with very disparate concentrations between initial years and producing increasing similar concentration patters between later years. The results of a 5-year run with seed concentrations listed in

Table 3 show annual blooms and nutrient concentrations (Figure 15) that are more repetitive than the optimal simulation results (Figure 14).

It is important to maintain a minimum population of MR in the estuary or in the coastal water out the estuary to facilitate bloom initialization over several years. The minimum concentration of MR mimics the process of cells entering the estuary from the ocean or lateral bays. A three-dimensional model would address the uncertainties of seed population origin; however, in this simple one-dimensional model the concentrations are maintained at levels that allow the blooms to be reproduced annually from August to October. A change in minimum concentration produces a response similar to a change in nitrogen uptake rate or maximum CR cell absorption limit. As the minimum concentration is raised, more MR cells are present in the estuary to bloom rapidly but also deplete CR populations rapidly. This has a dampening effect on the populations of CR and MR in the estuary when the parameters force low concentrations. Figure 16 shows the effect of imposing a minimum MR concentration on surface concentrations.

Table 3: Component seed concentrations for Figure 15.

Initial Seed Concentration [mmol N/ m^3]				
MR	**CR**	**NO$_3$**	**NH$_4$**	**Detritus**
0.01	1×10^{-10}	35.065	0.0058	1×10^{-10}

(a) MR

(b) CR

(c) NO$_3$

(d) NH4

(e) Detritus
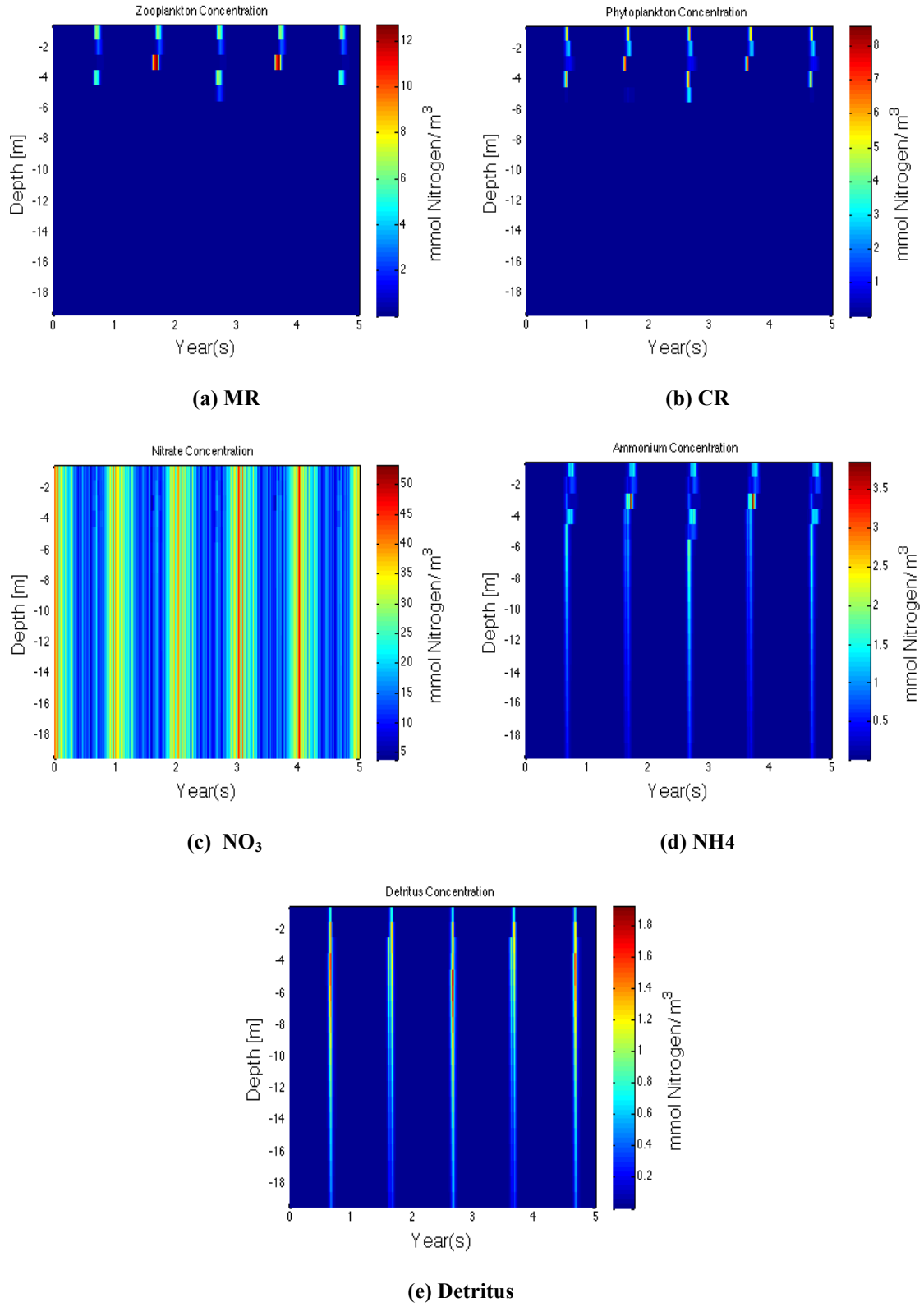
**Figure 15:** Nutrient and biological concentrations that produce similar yearly patterns through the water column from seed concentrations listed in Table 3 and parameters listed in Table 1.
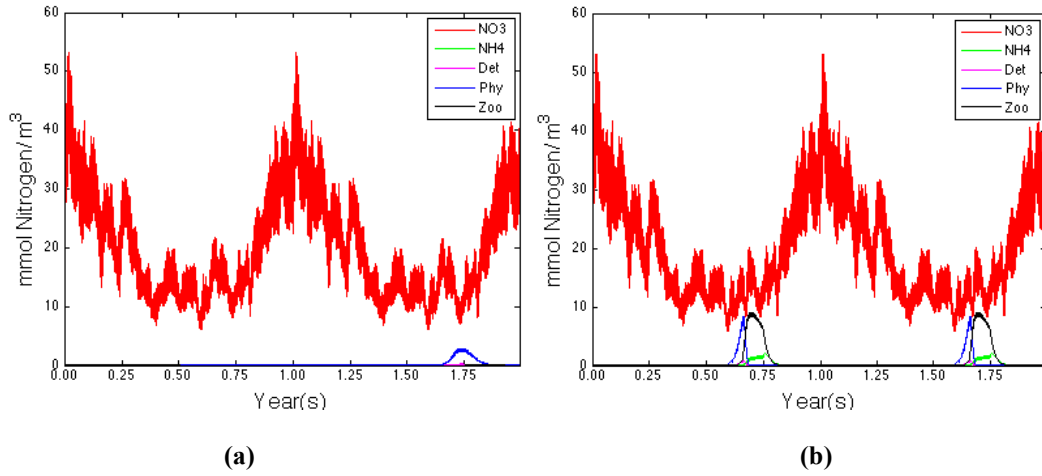
Figure 16: (a) Surface concentrations over two years with the initial seed concentrations in Table 3 and without minimum concentrations. **(b)** Surface concentrations over two years with the same seed concentrations and a minimum concentration of 0.01 mmol N m^{-3} for MR.

3.7 Vertical Migration

MR possess an essential survival skill: the ability to swim up to 1.2 cm s^{-1} (Hansen and Fenchel, 2006). This means that MR do not behave like passive particles in the dynamic estuary environment. The ciliates are capable of swimming away from the surface when a strong flux threatens to flush them out of the estuary, then return to the surface to continue photosynthesis and grazing. The current model contains an adjustable swimming speed ($swim_{max}$). The speed is the amplitude of the periodic swimming velocity calculated from Equation 6, a simplified equation derived from the tidal frequency and phase. Figure 17 illustrates the sensitivity analysis of CR/MR biomass and nutrient concentrations at the surface and MR biomass at depth in the presence of a changing maximum swim speed ($swim_{max}$).
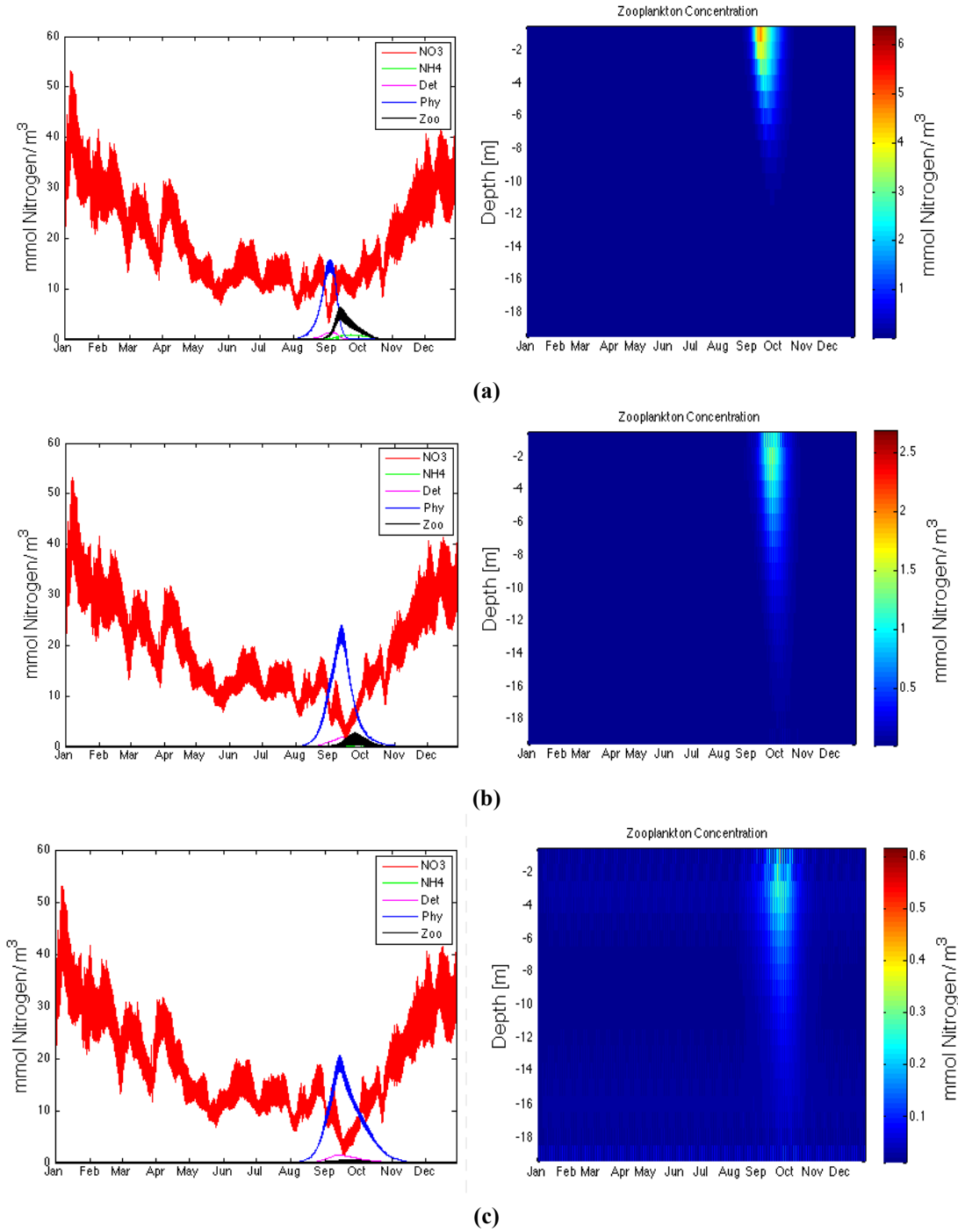
Figure 17: (Left) Surface level concentrations over one year with optimal simulation parameters and (right) MR concentrations throughout the column over time. The parameter $swim_{max}$ had the following values each run: **(a)** $swim_{max}$ = 0.035 mm/s, **(b)** $swim_{max}$ = 0.135, **(c)** $swim_{max}$ = 0.235,

(d)
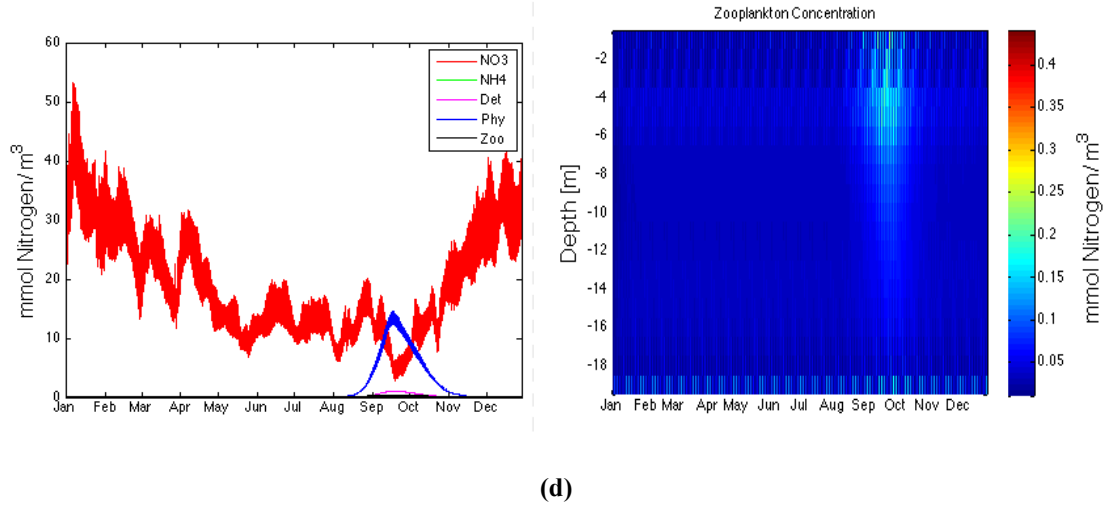
Figure 17 (continued): and **(d)** $swim_{max}$ = 0.335. The variable $swim_{max}$ (mm/s) controls vertical

migration . In the optimal simulation, $swim_{max}$ = 0.

As $swim_{max}$ increases by intervals of 0.1, the MR bloom peaks decrease. The most

dramatic decrease occurs between $swim_{max}$ = 0.035 mm/s and $swim_{max}$ = 0.135 mm/s,

with a decrease of approximately 3 mmol N/m^3 between MR peaks at the surface. MR

biomass also increases near the bottom as the swimming speed increases, especially in

the case of a maximum swimming speed of 0.335 mm/s. This would also mean that the

population is more spread over the water column. In the estuary, MR can jump and

change course in response to the environment; however, in this model the velocity

calculation is based on M2 tides and does not allow fluctuation in response to the

environment. As a result, organism exposure to beneficial resources such as light and

prey (highest concentrations at the surface) is reduced, and the total MR population

decreases in the presence of increasing maximum swimming speed. The only benefit MR

has to gain from vertical migration in this model is to escape the effects of flushing by

swimming to a depth that contains relatively stagnant water.

This simple, one dimensional model could not retain MR in the presence of advection when MR and CR advection were calculated similarly to nitrate advection (Equation 15, Appendix A) and fluxes were uniform over the vertical. MR was unable to sustain any bloom in the presence of advection due to flushing; however, a CR bloom could be observed at the surface because CR growth was able to outcompete the effects of advection by relatively high growth rates. The simulation was then modified to advect only the top half of the estuary column while the bottom half remained stationary with supplementary MR cell concentrations from the ocean. If it had the correct vertical migration pattern, theoretically MR would be able to swim to the stagnant level of water while high river fluxes drove advection at the surface, after which the cells could return to the surface to photosynthesize. Unfortunately, MR could not escape the effects of flushing in this scenario either.

Two obstacles prevent the simulation from effectively modeling an MR bloom in the presence of advection with the aid of vertical migration. First, the current optimal simulation parameters restrict the maximum swimming speed of MR. If MR swims too quickly, it spends so little time at the surface of the estuary that it is unable to photosynthesize. This reduces the overall population of MR in the water column. Second, the current advection model is such that MR cannot escape flushing by swimming to a different depth as the advection is uniform on the vertical. In order to test the swimming part of the model, a more sophisticated advection profile would be required so that a different flux could be imposed at each depth in a given time. Additionally, the

simulation could be expanded to a three-dimensional model that provides lateral bays to aid MR, CR, and nutrient retention, as lateral bays experience lower velocities and transport than the channels.

4. Conclusion

Sensitivity analysis of the optimal one-dimensional NNPZD model illustrates a dynamic relationship between MR, its prey CR, and effects on the biogeochemistry of the estuary over multiple years. Most of the parameters are positively correlated with the MR and CR bloom timing, duration, and peak. This includes maximum uptake rates, photosynthesis rates, seed concentrations, and MR vertical migration. Due to the MR photoautotrophy dependence on their prey, parameters related to CR have the strongest impact on the MR bloom. An optimal simulation setup was successfully parameterized with respect to nitrate advection, MR and CR maximum uptake rates, MR and CR mortality rates, MR photosynthesis rate, and minimum concentrations. Vertical migration and the advection of MR and CR were also explored. However, many uncertainties remain in constraining parameters, some of which significantly influence the MR bloom. The areas detailed below should be explored further in future MR modeling studies.

The sensitivity of the MR bloom to grazing through photosynthesis (the current model) in comparison to photosynthesis without grazing should be tested. The result could buoy CR populations, which may extend MR blooms or trigger MR blooms earlier in the subsequent cycle. It is expected that the difference in maximum MR population during a

cycle would be negligible. Photosynthesis is the primary contributor to MR growth and the driving force for high MR concentrations.

Maximum uptake rates were tested, but the P-I curve might also be important. The expectation is that changes in the P-I curve will produce the same results as changes in the uptake rates. The P-I curve is directly involved in the light limitation calculation (Equation 12 in Appendix A), which in turn is used to calculate MR and CR photosynthetic growth. If the P-I curve has a similar relationship to photosynthetic growth as nutrient uptake, the simulation may be equally sensitive to changes in the initial slope of the P-I curve as it is to the uptake rates. Little is known with respect to the photosynthesis rate of MR in the Columbia River estuary compared to other strains such as the Antarctic species (Johnson et al., 2006). Therefore testing the sensitivity of MR to parameters that are known to affect photosynthesis may yield some insights into the organism and its relationship with the estuary.

Future work should also allow the fluxes from the ocean and river to the estuary to be vertically variable so the water column can mimic the depth-dependent effect of the tides (flood and ebb). This would present a more realistic representation of advection, and provide a means to test MR retention time due to vertical migration in the presence of advection. A sensitivity analysis of the swimming speed, migration cycle between the surface and bottom of the water column, and fluxes with and without MR concentration in the ocean should be conducted and compared to observed data in the Columbia River estuary. The use of a two-dimensional channel representing the main channel of the

estuary might be a first approach to test the vertical migration speed with short enough simulations to perform sensitivity analyses.

Finally, it is recommended that oxygen be added to the model to assess the impact of MR on the oxygen cycle in the estuary. This is of special interest to local fishing businesses and environmental groups because of the sensitivity of some species, such as salmon, to oxygen concentration in the water. At this time, it is known that oxygen concentration changes in response to both consumption and production by MR and CR. Preliminary simulation runs with oxygen were calculated using Equation 9 (Appendix A). This equation subtracts respiration of CR and MR from the production of oxygen in the estuary with an air-sea interaction component. The calculation depends on the same parameters as the rest of the model, which means that oxygen is controlled by the same processes that have been addressed in the sensitivity analysis. The results of preliminary oxygen simulation experiments illustrate an increase of oxygen concentration from baseline values between August and October in the Columbia River estuary due to MR and CR photosynthesis during blooms. This trend has been observed in the Columbia River estuary, and further testing may clarify the relationship between oxygen and other elements of the NNPZD network.

References

Adolf et al. (2006) The balance of autotrophy and heterotrophy during mixotrophic growth of *Karlodinium micrum* (Dinophyceae), Journal of Plankton Research, 28: 737-751.

Barth, J. A. and Wheeler, P.A. (2005) Introduction to special section: Coastal Advances in Shelf Transport. Journal of Geophysical. Research. 110(C10), C10S01, doi:10.1029/2005JC003124.

Cloern, J. E. (1991) Tidal stirring and phytoplankton bloom dynamics in an estuary. Journal of Marine Research 49: 203–221.

Crawford et al. (1997) Recurrent Red-tides in the Southampton Water Estuary Caused by the Phototrophic Ciliate Mesodinium rubrum. Estuarine, Coastal and Shelf Science, 45: 799–812.

Garcia-Cuetos et al. (2012) Studies on the genus Mesodinium II. Ultrastructural and molecular investigations of five marine species help clarifying the taxonomy. Journal of Eukaryote Microbiology, 59: 374-400.

Hansen et al. (2013) Acquired phototrophy in Mesodinium and Dinophysis – A review of cellular organization, prey selectivity, nutrient uptake and bioenergetics. Harmful Algae, http://dx.doi.org/10.1016/j.hal.2013.06.004

Hansen, P. J. and Fenchel, T. (2006) The bloom-forming ciliate Mesodinium rubrum harbours a single permanent endosymbiont. Marine Biology Research, 2: 169-177.

Herfort et al. (2011*) Myrionecta rubra* population genetic diversity and its cryptophyte chloroplast specificity in recurrent red tides in the Columbia River estuary. Aquatic Microbial Ecology. 62

Herfort et al. (2012) Red waters of *Myrionecta rubra* are biogeochemical hotspots for the Columbia River estuary with impacts on primary/secondary productions and nutrient cycles. Estuaries and Coasts, 35: 878-891, DOI 10.1007/s12237-012-9485-z

Ivlev, V. S. (1961) Experimental ecology of the feeding of fishes. Yale University Press, New Haven, Connecticut, USA.

Johnson, M.D. and Stoeker D.K (2005) Role of feeding in growth and phytophysiology of *Myrionecta rubra*. Aquatic Microbial Ecology, 39:303-312.

Johnson et al. (2006) Sequestration, performance, and functional control of cryptophyte plastids in the ciliate *Myrionecta rubra* (*ciliophora*). Journal of Phycology, 42: 1235–1246.

Johnson et al. (2007) Retention of transcriptionally active cryptophyte nuclei by the ciliate *Myrionecta rubra*. Nature, 445: 426-428.

Kim et al. (2008) Growth and grazing responses of the mixotrophic dinoflagellate Diophysis acuminata as functions of light intensity and prey concentration. Aquatic Microbial Ecology, 51: 301-310.

Lindholm T. (1985), *Mesodinium rubrum* – a unique photosynthetic ciliate. Advances in Aquatic Microbiology, 3: 1-48.

Michaelis, L. and Menten, M.L. (1913). Die Kinetik der Invertinwirkung. *Biochem Z,* 49: 333–369

Peterson et al. (2013) Associations between *Mesodinium rubrum* and cryptophyte algae in the Columbia River estuary. Aquatic Microbial Ecology. 68(2)

Peterson et al. (2012) Red waters of *Myrionecta rubra* are biogeochemical hotspots for the Columbia River estuary with impacts on primary/secondary productions and nutrient cycles. Springer Link, 35: 878-891.

Spitz, Y. H. et al. (2005) Modeling of ecosystem processes on the Oregon shelf during the 2001 summer upwelling, J. Geophys. Res., 110, C10S17, doi:10.1029/2005JC002870.

Spitz, Y.H. (2011) Ecosystem Modeling of the Oregon Shelf: Everything but the Kitchen Sink. *Interdisciplinary Studies on Environmental Chemistry—Marine Environmental Modeling & Analysis*, Eds., K. Omori, X. Guo, N. Yoshie, N. Fujii, I. C. Handoh, A. Isobe and S. Tanabe, pp. 1–9

Spitz, Y.H. et al. (2015) Study of the Formation, Retention and Ecological Impact of a *Mesodinium* Bloom in the Columbia River Estuary – A model approach, In preparation.

U.S. Bureau of Reclamation, U.S. Army Corp of Engineers, and Bonneville Power Administration. (2001) The Columbia River System: The Inside Story. 2: 1-80

Wilkerson, F. P. and Gruneisch G. (1990) Formation of blooms by the symbiotic ciliate *Mesodinium rubrum:* the significance of nitrogen uptake. Journal of Plankton Research, 12: 973-989.

Yih et al. (2004) Ingestion of cryptophyte cells by the marine photosynthetic ciliate *Mesodinium rubrum.* Aquat. Microb. Ecol., 36: 165-170.

Zhang, Y. and Baptista, A. M. (2008) SELFE: A semi-implicit Eulerian–Lagrangian finite-element model for cross-scale ocean circulation. Ocean Modeling. 21(3-4): 71-96.
Appendices

A. Functions used in the model equations

• Nitrate and ammonium uptake was calculated using the classical Michaelis-Menten formulation (Michaelis and Menten, 1913).

$$uptakeN = \frac{V_M \times N}{K_s + N} \qquad (A1)$$

where V_M is the maximum uptake rate and K_s is the concentration at ½ V_M.

• Ivlev grazing was used to describe the consumption of phytoplankton (CR) by zooplankton (MR) (Ivlev, 1961).

$$graz = r_M \times [1 - e^{-\lambda P}] \qquad (A2)$$

where r_M is the maximum grazing rate, and λ is the Ivlev constant. P is the phytoplankton concentration.

• The light limitation function is defined as

$$lightlim = \frac{\alpha I}{\sqrt{V_M^2 + \alpha^2 I^2}} \qquad (A3)$$

where

$$I(z,t) = I_0 \exp \left(k_w z + k_p \int_z^0 CR(z') \, dz' + k_z \int_z^0 MR(z') \, dz' \right)$$

is the solar radiation, α is the initial slope of the P-I curve, and V_M is the maximum uptake rate. k_w, k_p and k_z are the coefficient of light attenuation by seawater, cryptophyte and *Mesodinium rubrum.* I_0 is the surface radiation obtained from the 2001 solar radiation

measurements at a mooring off Newport, Oregon, during the Coastal Ocean Advances in Shelf Transport (COAST) program (Barth and Wheeler, 2005). This includes the daylight cycle.

- The temperature limitation was defined to represent the seasonal variability of the temperature in the Columbia River estuary and favor growth during the warm period of summer-early fall (Figure 18).

$$
\begin{aligned}
templim = 0.75 + 0.1 \times \tanh\left[0.00055 \times \left(\left[1 - \frac{224}{dt}\right] + \frac{44}{dt}\right)\right] \\
+ 0.1 \times \tanh\left[-0.00055 \times \left(\left[1 - \frac{224}{dt}\right] - \frac{44}{dt}\right)\right]
\end{aligned}
\tag{A4}
$$

where the tanh function produces the curve in Figure A1.
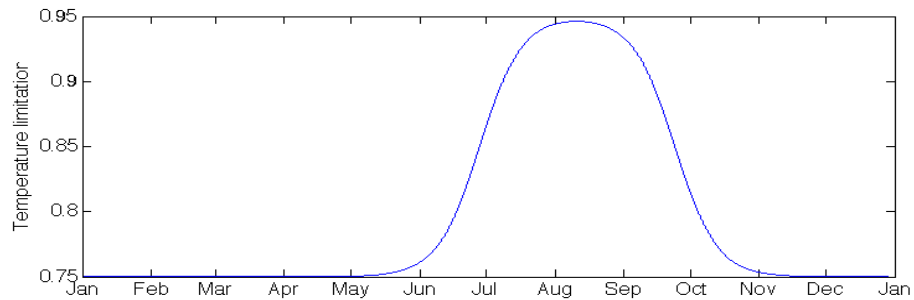
Figure A1: Function to limit MR and CR growth during cold seasons.

- The advection of nitrate is defined from the fluxes and concentrations from the river and ocean sides into the domain and from the modeled nitrate to the ocean and river.

$$AdvecNO_3 = FlowRiverIn * ConcRiver + FlowRiverOut * NO_3 \qquad (A5)$$
$$- FlowOceanIn * ConcOcean - FlowOceanOut * NO_3$$

where *FlowRiverIn* is the flux of water from the river source into the estuary, *FlowRiverOut* is the flux of water from the estuary into the river, *FlowOceanIn* is the flux of water from the ocean source into the estuary, *FlowOceanOut* is the flux of water from the estuary into the ocean, *ConcRiver* is the concentration of NO_3 in the river source, and *ConcOcean* is the concentration of NO_3 in the ocean source.
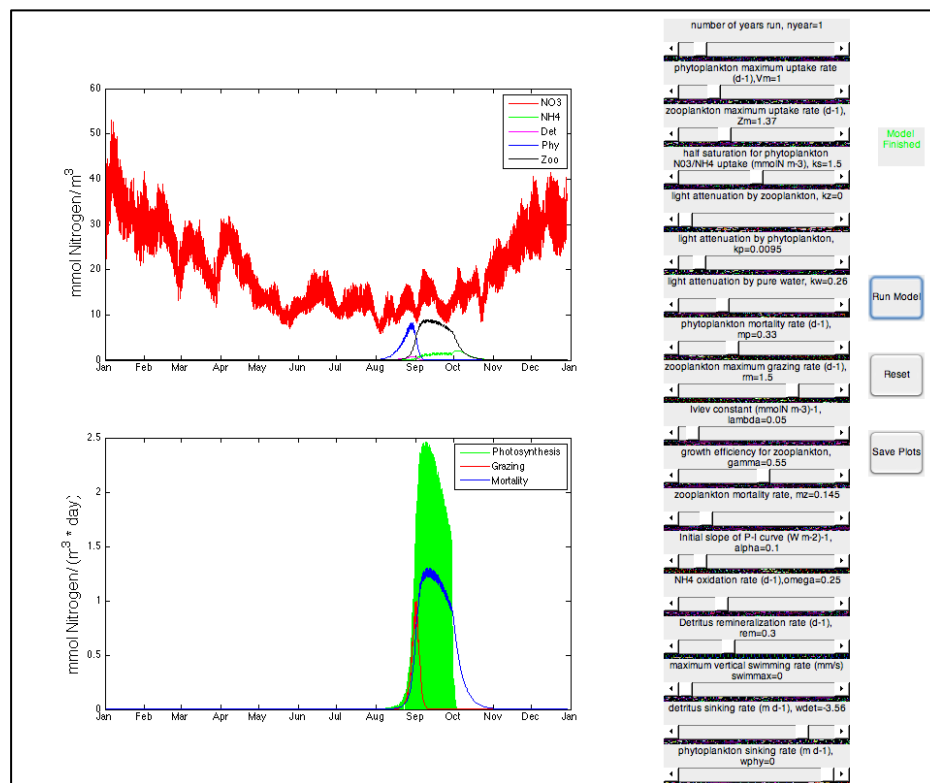
- Oxygen changes over time due to the biological sink (respiration) and source (production) and air-sea fluxes. The biological sources and sinks only are represented here.

$$\frac{\partial O}{\partial t} = r_{O_2NO_3} \times (uptakeNO_3 + lightlim \times templim \times CR + uptakeNO_3 \times lightlim \qquad (A6)$$
$$\times templim \times photopop \times MR) - 2 \times \Omega \times NH_4 + r_{O_2NH_4} \times (uptakeNH_4$$
$$+ lightlim \times templim \times CR + uptakeNH_4 \times lightlim \times templim \times photopop \times MR$$
$$- mz \times MR - rem \times D)$$

where r_{O2NO3} is the stoichiometric ratio of O_2:NO_3 and r_{O2NH4} is the stoichiometric ratio of O_2:NH_4.

B. MATLAB Graphical User Interface (GUI)

The model equations were solved in MATLAB as it is feasible for the simple one-dimensional setting of the performed simulations. A GUI interface (Figure B1) was designed such that the model parameters could easily be changed within a biological acceptable range. The side sliders allow the users to perform that task without editing the whole model code. In addition, the time evolution of the CR and MR bloom, of the nutrient concentration and of the main pathways that lead to the MR bloom (photosynthesis, grazing and mortality) is instantaneously visualized.

Figure B1: MATLAB GUI interface**.**